TENSEGRITY BASED PROBES FOR PLANETARY EXPLORATION: ENTRY, DESCENT AND LANDING (EDL) AND SURFACE MOBILITY ANALYSIS

Vytas SunSpiral[1], George Gorospe[2], Jonathan Bruce[3], Atil Iscen[4], George Korbel[5], Sophie Milam[6], Adrian Agogino[7], and David Atkinson[8]

[1]*SGT Inc., NASA Ames Research Center, Moffet Field, CA, 94035, USA, vytas.sunspiral@nasa.gov*
[2]*USRA, NASA Ames Research Center, Moffet Field, CA, 94035, USA, george.e.gorospe@nasa.gov*
[3]*USRA/UC Santa Cruz, NASA Ames Research Center, Moffet Field, CA, 94035, USA, jbruce@soe.ucsc.edu*
[4]*Oregon State University, Corvallis, OR, 97331, USA, iscena@onid.oregonstate.edu*
[5]*University of Idaho, Moscow, ID, 83844, USA, korb6243@vandals.uidaho.edu*
[6]*University of Idaho, Moscow, ID, 83844, USA, mila0725@vandals.uidaho.edu*
[7]*UC Santa Cruz, NASA Ames Research Center, Moffet Field, CA, 94035, USA, adrian.k.agogino@nasa.gov*
[8]*University of Idaho, Moscow, ID, 83844, USA, atkinson@uidaho.edu*

ABSTRACT

In this paper we evaluate tensegrity probes on the basis of the EDL phase performance of the probe in the context of a mission to Titan. Tensegrity probes are structurally designed around tension networks and are composed of tensile and compression elements. Such probes have unique physical force distribution properties and can be both landing and mobility platforms, allowing for dramatically simpler mission profile and reduced costs. Our concept is to develop a tensegrity probe in which the tensile network can be actively controlled to enable compact stowage for launch followed by deployment in preparation for landing. Due to their natural compliance and structural force distribution properties, tensegrity probes can safely absorb significant impact forces, enabling high speed Entry, Descent, and Landing (EDL) scenarios where the probe itself acts much like an airbag. However, unlike an airbag which must be discarded after a single use, the tensegrity probe can actively control its shape to provide compliant rolling mobility while still maintaining its ability to safely absorb impact shocks that might occur during exploration. (See Figure 1) This combination of functions from a single structure enables compact and light-weight planetary exploration missions with the capabilities of traditional wheeled rovers, but with the mass and cost similar or less than a stationary probe. In this paper we cover this new mission concept and tensegrity probe technologies for compact storage, EDL, and surface mobility, with an focus on analyzing the landing phase performance and ability to protect and deliver scientific payloads. The analysis is than supported with results from physical prototype drop-tests.

Key words: Tensegrity, Titan, EDL, Rover.

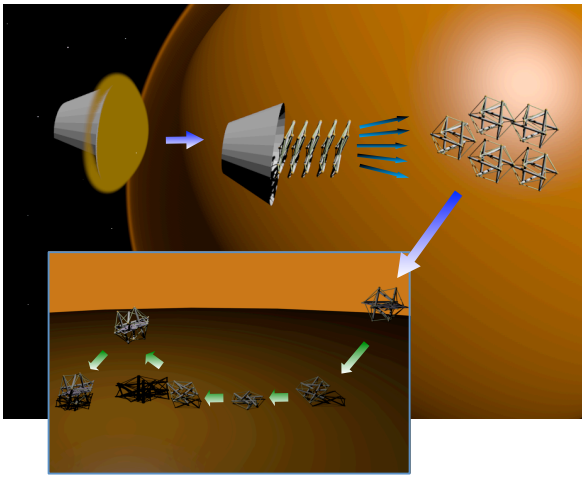

Figure 1: *Tensegrity structures are composed of pure compression and tension elements. They can be lightweight, reliable, deployable, and efficient to manipulate.* **Mission Scenario** - *Tightly packed set of tensegrities, expand, spread out, fall to surface of moon, then safely bounce on impact. The same tensegrity structure which cushioned the landing is then used for mobility to explore moons such as Titan and small asteroids.*

1. INTRODUCTION

In this paper we evaluate tensegrity probes on the basis of the EDL phase performance of the probe in the context of a mission to Titan. Titan's atmosphere, stable bodies of surface liquid and complex organics make it one of the most complex and Earth-like environments in the solar system. This tensegrity probe mission will build on the science returns from Huygens and answer many of the new and unresolved questions surrounding Titan's ongoing organic processes, geologic history, atmosphere, and surface-atmosphere interactions. As shown in Figure

1, upon arrival at Titan, the tightly packed tensegrity probes will separate from the spacecraft and expand to fully deployed shock absorbing state. Without requiring parachutes, each probe is projected to impact the surface at about 11 m/s, absorbing and distributing impact stresses while protecting its science payload, much like an air-bag. As the tensegrity probes bounce, roll, and finally come to a rest on the surface of Titan, the actuated tensegrity structure will then begin to function as the primary mobility system for these mobile probes, enabling surface exploration. Once on the surface, a notional science payload containing an atmospheric package, an analytical chemistry package, and an imaging package can begin the probes' science mission.

An individual tensegrity probe has a significantly lower EDL hardware overhead and increased science payload mass percentage when compared to similar planetary surface rover missions, increasing the potential for science return. We evaluate this by comparing the total system mass at the point of atmospheric entry with the mass of the rover's productive payload, which constitutes all the science instruments and associated avionics, power, and controllers. Compared with the Mars Exploration Rovers (MER) and Mars Science Laboratory (MSL) which had a science payload mass fraction of 18% for MER and 22% for MSL, we show in this paper that a tensegrity probe may be able to operate on Titan as a mobile probe with a science payload mass fraction of 50% due to the dual use of the tensegrity structure as for both EDL and surface mobility. Further analysis may drive this percentage higher as more efficient versions of the tensegrity lander are explored and when they are considered in the context of a multi-probe mission enabled by their lightweight and compact storage. By increasing the mass ratio of productive science payload vs total system mass, this approach helps drive down future mission costs by allowing smaller lighter missions with the full capabilities of EDL and surface mobility.

In this paper will will start with background material on tensegrity structures (Section 2), and discuss how they can be used as planetary exploration probes. Next we will describe our notional mission to Titan (Section 3), which we use to drive our engineering development of the concept, and compare our approach to flown missions by comparing the fraction of system mass that can be dedicated to the scientific payload. In Section 4 we use two different simulation approaches to analyze the probes response to landing events, and evaluate structural design choices to manage payload deceleration forces. In Section 5 we examine the results of physical prototype drop tests which show initial validation of the concept. Finally, in Section 6, we give a brief overview of our surface mobility control methods, which have been extensively reported on in other papers.

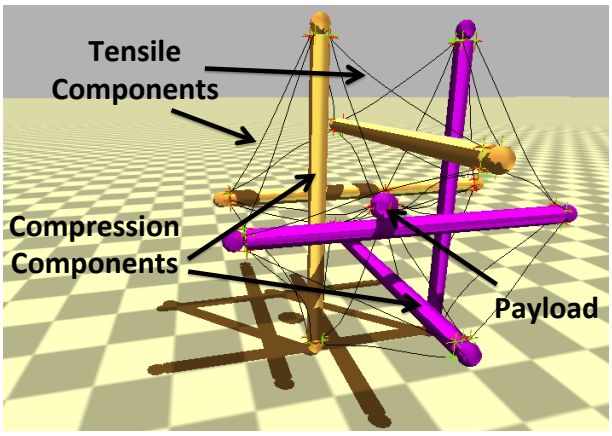

Figure 2: **Tensegrity Structure.** *Tensegrities are composed of pure tension and pure compression elements (e.g. cables and rods) as seen in this picture of a tensegrity robot from our physics based tensegrity simulator. They are light-weight, energy-efficient and robust to failures.*

2. TENSEGRITY BASED PROBES

2.1. Introduction to Tensegrity Structures

Within the exciting and emerging field of soft-body robotics is the subset of Tensegrity robotics which are composed of pure tension and compression elements (usually cables and rods - see Figure 2). These structures are made of axially loaded compression elements encompassed within a network of tensional elements, and thus each element experiences either pure linear compression or pure linear tension [9]. As a result, individual elements can be extremely lightweight as there are no bending or shear forces that must be resisted, due to their unique property of internally distributing forces, which prevents these forces from magnifying into joints or other common points of failure. Rather, externally applied forces distribute through the structure via multiple load paths, creating a system level robustness and tolerance to forces applied from any direction. Therefore, tensegrity structures can be easily reoriented and are ideally suited for operation in dynamic environments where contact forces cannot always be predicted. Likewise, tensegrities can be robust to the failure of individual actuation elements, resulting in a gradual reduction of overall workspace, rather than the loss of entire ranges of motion which are common in serial manipulators.

Tensegrity structures are a fairly modern concept, having been founded by the artist Kenneth Snelson [50, 49] in the 1940's and initially explored for architecture in the 1960's by Buckminster Fuller [11]. In the 1970's, a formal definition for a tensegrity structure was defined as a set of discontinuous compressive elements interacting with a set of continuous tensile elements which maintain a stable volume in space [39]. For the first few decades, the majority of tensegrity related research was concerned with form-finding techniques [55, 27, 51, 56]

and the design and analysis of static structures [38, 9, 52]. Research into control of tensegrity structures was initiated in the mid-1990's, with initial efforts at formalizing the dynamics of tensegrity structures only recently emerging [54, 47, 48]. The very properties that make tensegrities ideal for physical interaction with the environment (compliance, multi-path load distribution, nonlinear dynamics, etc) also present significant challenges to traditional control approaches. A recent review [54] shows that there are still many open problems in actively controlling tensegrities. We believe that modern control algorithms based on central pattern generators and distributed reinforcement learning will be key elements in controlling tensegrity robots.

Use of tensegrity robots for mobility was initiated in 2004-6 by papers from Masic [28], Aldrich [3], and Paul [36, 37]. As a result of studies showing the prevalence of tensegrity structures in nature such as cell structure [15] and anatomy [23, 40], and the challenges of controlling tensegrity structures using traditional approaches, the majority of the works in mobile tensegrity robotics have shown biological inspiration in their motivation, using evolutionary algorithms [35, 36, 37, 41, 42, 43, 17], neuroscience inspired CPGs [53, 6, 4, 5], and biomimetic structures such as manta-ray wings [30], or caterpillars [42, 34, 32, 33]. See also [44, 45, 20, 7, 29] for other works on the locomotion of tensegrity robots. To the authors knowledge, this work is the first to explore tensegrity structures for use as planetary probe landing systems.

2.2. Benefits of Tensegrity Structures

Tensegrities have a number of beneficial properties including:

- **Light-weight**: Forces align axially with components and shocks distribute through the tensegrity, allowing tensegrities to be made of light-weight tubes/rods and cables/elastic lines.
- **Compact Storage**: Tensegrity structures can be packed into compact forms for launch and deployed to a functional configuration prior to landing. This deployment uses the same actuation system that will later provide mobility.
- **Energy efficient**: Through the use of elastic tensile components and dynamical gaits, efficient movement is possible.
- **Robust to failures**: Tensegrities are naturally distributed systems and can gracefully degrade performance in the event of actuation or structural failure.
- **Capable of unique modes of locomotion**: Tensegrities can roll, crawl, gallop, swim or flap wings depending on construction and need.
- **Impact tolerant and compliant**: Since forces are distributed upon impact, they can fall or bump into things at moderate speed. In addition, their compliance ensures that they do minimal damage to objects they contact.
- **Naturally distributed control**: Characteristics of force propagation in tensegrities allows effective local controllers.

The last property is the most subtle but important. In "traditional" robots, distributed controls becomes messy due to the need to communicate global state information to all the controllers with high precision, and thus often undermines the very promise of distribution. Fundamentally, this stems from the fact that a rigidly connected structure will magnify forces internally through leverage, and will accumulate force into joints. Thus, the actions of a local distributed controller can have disproportionate global consequences. These consequences can require a certain amount of global coordination and state management, undermining the value of the local controller. Tensegrity structures are different, due to the tension network, there is no leverage in the structure. Thus, forces *diffuse* through the structure, rather than accumulate in joints. As a result, actions by a local controller diffuse through the structure, integrating with all the other local controllers. While any one local controller will impact the structure globally, that impact is locality relevant and not magnified via leverage. Thus, the structure enables true distributed control, because local actions stay (predominately) local.

Despite these desirable properties, tensegrity robots have remained mostly a novelty for many years due to difficult control properties that make them hard to control with traditional control algorithms such as:

1. **Complex oscillatory motions**: Tensegrity robots tend to have oscillatory motions influenced by their interactions with their environment.
2. **Elastic Nonlinear distributed interactions**: A force generated on one part of the tensegrity propagates in a nonlinear way through the entire tensegrity, causing shape changes, which further change force propagations.

Fortunately the combinatorial optimization capabilities of evolutionary algorithms combined with the distributed properties of multiagent systems are a natural match to these problems. Evolutionary algorithms can learn complex control policies that maximize a performance criterion without needing to handle the oscillatory motions and distributed interactions explicitly. In addition, increased performance can be achieved by assigning evolving agents to different control points throughout the tensegrity. Then as a multiagent system, the agents can co-evolve to create a unified control policy.

2.3. Compact Storage and Deployment

The six bar icosahedron tensegrity structure used as a basis for the tensegrity probe is capable of collapsing down

to a base shape of an isosceles triangle with side lengths equal to the length of the struts and a height of about three times the diameter of the struts. Simulation has shown that the structure can collapse itself to this configuration by manipulating all 24 of its tension members with half of the tension members fully shortened and the other half fully lengthened (figure 3).

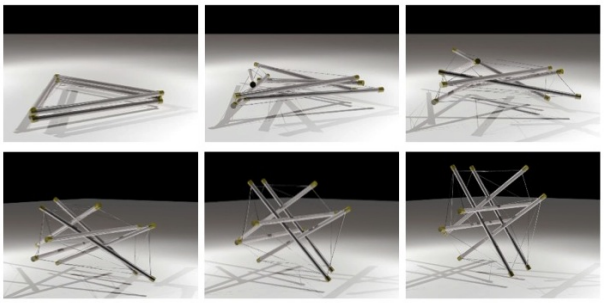

Figure 3: **Deployment** *The six bar tensegrity probe can be packed into a flat triangle and then deployed to full functional configuration by changing the string lengths with the same actuators which will be used later for mobility.*

3. TITAN MISSION DESIGN

3.1. Titan Mission Narrative

An ambitious tensegrity based probe mission to Titan would seek to answer many of the primary questions regarding the moon's surface chemistry, geology and meteorological properties through the delivery of the latest in-situ instruments to the surface. The innovative use of tensegrity structures to surround and shield the science payload during EDL advances this goal of delivering instruments to scientifically significant environments. Such a mission if launched in January, 2018 would arrive at the Saturn system within 10 years via Jupiter fly-by. The spacecraft, a Titan orbiter, will arrive at Titan traveling approximately 6.5 km/s. A tensegrity probe entry vehicle consisting of a heat shield, back shell, and a single light weight tensegrity probe stored in a space saving cruise configuration, will then be deployed from the orbiter and will enter the Titan atmosphere at 100,000 km above the surface. The entry vehicle will jettison the heat shield at 200 km above the surface. Based on simulations using the Titan atmospheric data collected by the Huygens probe in 2005, each spherical tensegrity probe of .863 diameter with a drag coefficient of 0.5 is expected to be traveling at a terminal velocity of 11.4 m/s before impact.

As the probe begins free descent, it will actuate its cable elements, increasing tension throughout the tensegrity structure causing it to expand from its flat triangular stored shape into its fully deployed and pre-tensioned spherical shape. The probe then commands each actuation element to engage brakes so that landing impact shocks do not reflect into the motors. The pre-tension state of the structure permits the full kinetic energy of the falling probe to be distributed through the structure. The cables, which have some elasticity, allow the structure to slightly deform from the impact stress, while the center slung payload safely decelerates to a full stop without impacting the surface. Following the probe's rebound off the surface and the eventual settling of the probe into a state of zero kinetic energy, the brakes can be released enabling the structure to move and reorient itself.

Tensegrity probe surface operations will rely heavily on the tensegrity structure for payload positioning and vehicle mobility. A mobile tensegrity probe on the surface of Titan will have the opportunity to seek out interesting sites to gather data and perform in situ investigations of the mineralogical content, organics, atmospheric and meteorological systems present on the icy moon. Whole segments of the surface operations will be devoted to acquiring samples, making measurements, and capturing images which will increase our knowledge and understanding of these scientific topics. Many particularly interesting geologic sites are also high risk sites due to limited reconnaissance and unknown soil properties, such as steep sand dunes or cliff faces. One of the advantages of a Tensegrity probe is that it can withstand a fall at Titan's terminal velocity, so it can survive falling off a cliff, or intentionally leaping into a cave or other scientifically interesting location. Unlike the Mars rovers, which discarded their airbags after landing, the probe's basic mobility system is also its landing system, available to protect it at any moment. This will enable mission operators to explore areas that are of high scientific interest, but which would be far too risky for a traditional rover. Surface mobility will be covered in Section 6.

3.2. Target Tensegrity Platform

The structure of the tensegrity used in this paper is shown in Figure 2. Rods do not connect directly with other rods, instead, rods are indirectly connected through cables, resulting in a continuous tension network as the primary load transfer system of the structure. In the orientation shown in Figure 2 one pair of the rods are parallel to x-axis, another pair is parallel to y axis and the last pair is parallel to z-axis. Each end of a rod is connected to the ends of other non parallel rods via 4 different cables. When the structure is in balance, it is symmetrical and convenient for a rolling motion. On the other hand, when an external force is applied, it easily deforms and distributes the force to every component of the structure.

In addition to the base tensegrity, we attached a ball shaped payload to the center of the tensegrity via an additional 8 payload cables. The payload represents the essential parts of the robot, such as computing, sensors, batteries, or other instruments. Just like the 24 outer cables, these 8 payload cables may be actively controlled depending on the control law being implemented. (Figures 2, 17). We found in our mobility studies that the actuated payload cables greatly improved rolling mobility, and enabled hill climbing, through active control of the center of mass of the structure.

For the tensegrity mission to be cost effective our overall weight must be low. Yet we must still have enough instruments for high scientific return. Our goal in instrument choices is to make a good balance between these competing requirements. Figure 4 shows the expected weight of the components of our mission, and the overall weight. The mass of this operational science payload is used to determine engineering aspects of the tensegrity structure parameters, mission design, and mission operational scenarios, such as actuator strength and material properties. The notional operational payload is estimated to be 70 kg, including science instruments and support avionics and power. Given the operational payload mass, the tensegrity support structure and its actuators which weigh approximately 30 kg combined, the entire vehicle is estimated be 100 kg.

Notional Mass Properties for a Tensegrity Probe:

Probe Subsystem:	(kg)
Tensegrity Structure and Actuation Hardware	30.0
Avionics	23.1
Communication	6.0
Electrical Power Subsystem	36.0
Imagery Package	0.7
Meteorology Package	1.4
Analytical Chemistry Package	2.8
Total	100.0

The notional scientific payload for a tensegrity probe mission will have three science packages:

Atmospheric and Meteorology Package:
- Temperature/Pressure
- Wind Speed/Direction
- Methane Humidity

Analytical Chemistry Package:
- Gas Chromatograph
- Mass Spectrometer

Imaging Package:
- Navigation Cameras
- Field Microscope

Figure 4: **Notional Mass Properties of a Tensegrity Probe**. *References: Avionics [8], Commmunications [8], Imagry Package [26, 14], Meterology Package [13], Analytical Chemistry Package [10].*

3.3. Tensegrity Probes in Comparison to Other Flown Missions

For more than 20 years NASA's Discovery program has funded low cost, highly focused missions demonstrating new technology and seeking out the answers to fundamental questions regarding solar system formation, potentially habitable environments, and potential locations within the solar system where life could begin and evolve. The program has many successes, amongst them the Mars Pathfinder mission which deployed a Mars rover called Sojourner, NASA's first rover on Mars [12]. A tensegrity based probe mission to Titan can be compared to other Discovery program missions due to it's demonstration of new EDL technology and focused science objectives. A primary goal of the mission is the demonstration and validation of the tensegrity structure as capable EDL equipment and primary mobility equipment. Using a tensegrity structure in this way enables the tensegrity probe to comprise a larger percentage of the entry mass than other missions such as Pathfinder, the Mars Exploration Rover missions, or the Mars Science Laboratory mission. When compared with the Mars Exploration Rovers which had an entry mass of 830 kg, of which 146 kg of equipment directly supported instrumentation and scientific study, the tensegrity probe represents the entirety of the planned landed mass and will not have to discard any hardware before initiating surface operations, other than a heat shield for initial entry. Based on Titan heat shield studies which show that it would be reasonable to assume 35-41% TPS/probe mass using PICA, Tufroc, or heritage SLA [21, 24], we assume 40kg of heat shields required for a single 100kg probe. After slowing to terminal velocity and discarding the heat shield, a tensegrity probe is capable of landing and carrying a center slung payload weighing as much as 70 kg as it travels across the surface of Titan. This payload will contain all science instruments and payload support equipment. Thus, as can be seen in Table 5, the tensegrity probe enables a mission to dedicate 50% of the entry mass to productive science equipment whereas Pathfinder delivered 1% science payload, MER's was 17%, and MSL provided 22% of its entry mass as productive payload. Since mass is a driving aspect of mission cost – driving everything from launch vehicle to the interplanetary vehicle and fuel requirements, we believe that enabling better science payload to entry system mass will help drive down future missions costs.

	Pathfinder	MER	MSL	Huygens	Tensegrity
Entry Mass (kg)	587	831	3301	320	140
Landed Mass (kg)	372	540	943	223	100
Rover Mass (kg)	11	175	943	0	100
Science Payload and Support Avionics (kg)	8	146	723	223	70
Productive Science Mass Percentage	1%	17%	22%	69.7% No Mobility	50%

Figure 5: **Planetary Exploration Missions by Mass**. *References: Pathfinder [31], MER [31], MSL [22], Huygens [8].*

4. STRUCTURAL ANALYSIS FOR ENTRY, DESCENT, AND LANDING

4.1. NTRT Tensegrity Simulator

To simulate landing and locomotion, we utilize the NASA Tensegrity Robotics Toolkit (NTRT), a tensegrity simulator developed in our lab which is based on the Bullet physics engine. We are in the process of releasing this as an open-source library and will post it's availability on the project website [1]. Bullet is an open source physics engine that does 3D collision detection, rigid and soft body dynamics in discrete time, though the NTRT does not use the soft body dynamics. For the tensegrity simulation, we use the rigid body collisions provided by Bullet for compressional elements (rods of the structure), and we added simulation of tensional elements (strings) using basic physics for elastic strings. To be able to simulate both rigid bodies and tensional elements together, at each time step, all the forces applied by the strings to the rods are calculated manually. These are then provided to the Bullet physics engine, and Bullet calculates the positions, orientations and velocities of all the rigid bodies considering previous states, tensional forces that we add, and possible collisions.

To simulate tensional forces, we use the rest length (L_R) and elasticity coefficient (c_e) of the strings that are defined as part of the material property. During the simulations, at each time step, the actual length (L_A) is extracted from Bullet, and if the string is stretched ($L_A > L_R$), the tensional force for each string is calculated using the elasticity formula $|F| = c_e * (L_A - L_R)$. On the other hand, if the string is slack ($L_A > L_R$) the force is accepted as zero (no compressional force caused by strings).

The resulting graphical illustration of the process is given by Figure 6. As it can be seen on the left, before the moment of impact, all the strings are equally stretched. On the other hand, after the impact, the payload moves down further stretching some of the strings and temporarily deforming the structure.

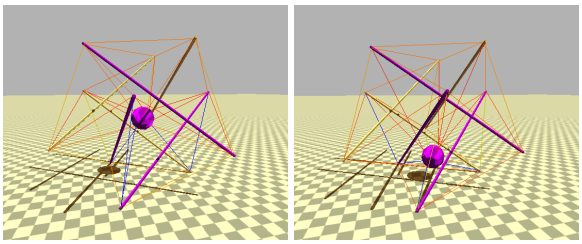

(a) Before Impact (b) After Impact

Figure 6: Snapshot of the landing simulations using the NASA Tensegrity Robotics Toolkit (NTRT). The strings are colored according to their stretch / tension. After the impact the payload moves down stretching strings and temporarily deforming the structure.

4.2. Landing Simulation using Euler-Lagrange Solver

In order to verify the simulation results produced by our NTRT simulator, we decided to compare the behavior of the NTRT to a published analytic model for tensegrity systems. We choose to use Skelton's dynamic equations found in his *Tensegrity Systems* book [47] which is based on his work in [46]. In order to easily solve the dynamic equations with interactions with the environment, an Euler-Lagrange approach is used as well as Skelton's constrained class 1 structure. The lagrange equation for a constrained rod is given by

$$L = T - V - c \tag{1}$$

where

$$\mathbf{b} = l^{-1}(\mathbf{n}_j - \mathbf{n}_i) \tag{2}$$

$$c = \frac{\mathbf{J}\xi}{2}(\mathbf{b}^T\mathbf{b} - 1) \tag{3}$$

Equation (2) is the normalized vector of a rod with $\mathbf{n}_{i,j}$ the nodal positions in R^3, and equation (3) contains the lagrange multiplier ξ to keep (2) constrained. $\mathbf{J}$ is also defined as the inertia matrix for a 1 dimensional rod in 3 dimensional space. In order to define the system of k rods we need to define a combined Lagrangian as

$$\mathbf{L} = \sum_{i=1}^{k} L_i \tag{4}$$

where L_i is the Lagrange function for each rod. Using the approach outlined in Skelton's book for deriving the equations of motion, we can then derive the configuration matrix

$$\mathbf{Q} = [\mathbf{R} \quad \mathbf{B}] \tag{5}$$

where $\mathbf{R}$ and $\mathbf{B}$ are matrices containing the translational and rotational vectors, respectively. They have the form

$$\mathbf{R} = [\mathbf{r}_1 \quad \cdots \quad \mathbf{r}_k] \tag{6}$$

$$\mathbf{B} = [\mathbf{b}_1 \quad \cdots \quad \mathbf{b}_k] \tag{7}$$

Also using the procedure to derive generalized forces within Skelton's book, the systems's generalized force equations are computed as

$$\mathbf{F_Q} = [\mathbf{F_R} \quad \mathbf{F_B}] \tag{8}$$

with

$$\mathbf{F_R} = [\mathbf{f}_{\mathbf{r}_1} \quad \cdots \quad \mathbf{f}_{\mathbf{r}_k}] \tag{9}$$

$$\mathbf{F_B} = [\mathbf{f}_{\mathbf{b}_1} \quad \cdots \quad \mathbf{f}_{\mathbf{b}_k}] \tag{10}$$

Finally, we can define the resulting equations of motion in a compact form as

$$(\ddot{\mathbf{Q}} + \mathbf{Q}\mathbf{\Xi})\mathbf{M} = \mathbf{F_Q} \tag{11}$$

where

$$\mathbf{\Xi} = diag\,[0, \cdots, 0, \xi_1, \cdots, \xi_k] \tag{12}$$

$$\mathbf{M} = diag\,[m_1, \cdots, m_k, J_1, \cdots, J_k] \tag{13}$$

This approach was then implemented in Python utilizing a 4th order Runge-Kutta formula for solving the system of ordinary differential equations. In order to implement a gravitational field, a force distribution function is applied along the length of each rod and calculated as a nodal force depending on the given density of the rod. This external force is then applied to the nodes during each time step, simulating a gravitational field.

4.3. Detailed Impact Simulations and Cross-Validation Using Two Simulators

We used these two simulators because they both have strengths and weaknesses. The NTRT simulator is the most general purpose, allowing us to explore control algorithms and complex environmental interactions, but it is an iterative discrete solver that we were concerned might not be providing accurate answers. The E-L solver, on the other hand, has a much stronger analytical basis and should provide very accurate answers, but is limited because some of the nodes (i.e. rod ends) must be constrained and locked into place. This is unrealistic for the deformation caused during landing, and makes it an inappropriate choice for mobility and controls research.

In this section, we compare the NTRT simulator and E-L solver at the moment of impact with the ground. The simulations are compared at the moment of impact with the ground because our implementation of the analytic E-L solver requires select nodes to be constrained. We setup the structure so that it is barely in contact with the ground and is in balance at time equal to 0. In both simulations, we add an initial velocity equal to the terminal velocity of Titan, and compared each vertical trajectory, vertical velocity, and vertical acceleration of the payload. Since the structures horizontal speed is zero at the beginning and the structure is symmetrical, the payload's horizontal components of position, velocity and acceleration are zero. As it can be seen in the Figures 7 and 8, both simulators closely match and generate the same results for position and velocity with the error margin close to zero. Comparing the accelerations generated by two simulators (Figure 9), it can be seen that there is a bigger difference. The reason behind this difference is the fact that NTRT uses Bullet, which is a discrete time simulator and accelerations are calculated using two point estimations from velocities at the timestep before. Yet, even with these differences in accelerations, our conclusion at the end of the comparison is that both simulators showed the same basic dynamics and their results were close enough that we could move forward using the more general purpose NTRT Simulator for our controls, mobility, and landing experiments.

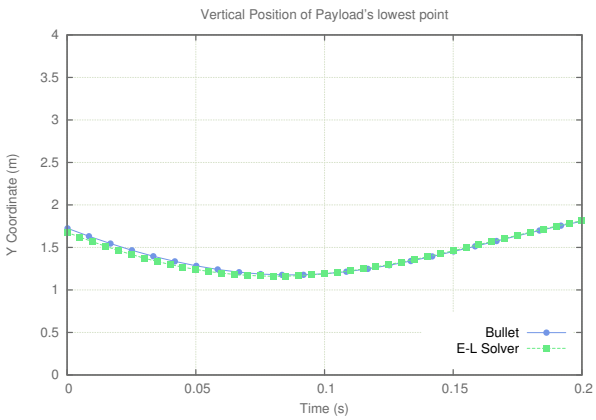

Figure 7: NTRT vs EL: Vertical Position

4.4. Simulated Drop Tests and Payload Protection

Finally, we performed extensive analysis on drop tests and the protection provided to a payload. As expected, we found that by varying the rod lengths, which impacts the stroke distance for the payload to decelerate, we could control the maximum deceleration experienced by the payload while ensuring that it did not collide with the ground or structure. For example, with rods of 1.5 meters in length, our payload experienced a max deceleration of 21.4G when landing at 15 m/s. In figure 10 we show the results of a series of drop tests with different rod lengths and show the resulting maximum deceleration and forces experienced in the tension members. As can be seen from these graphs, even for reasonable rod lengths,

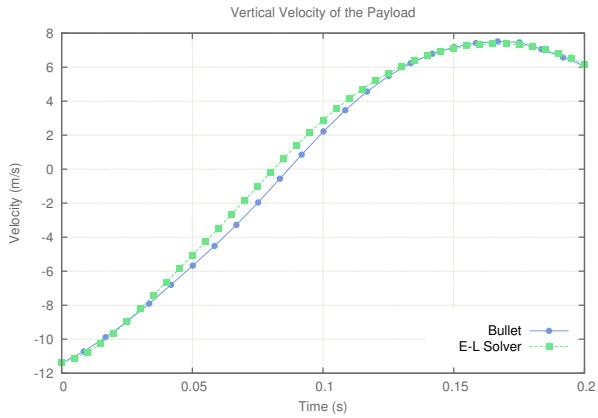

Figure 8: NTRT vs EL Vertical Velocity

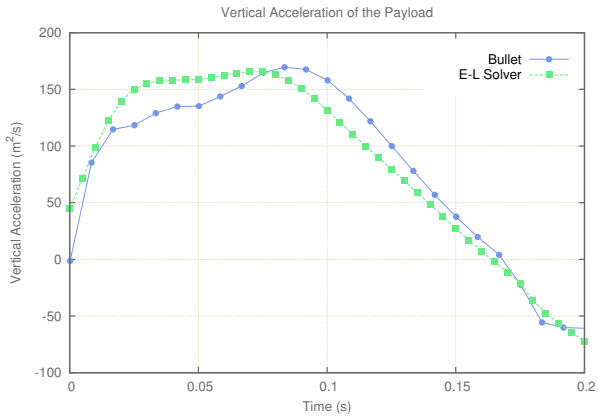

Figure 9: NTRT vs EL Vertical Acceleration

the maximum G's are acceptable for most instruments, and the maximum forces experienced by the cables are easily within ranges that can be engineered for. In all tests we kept the total system mass constant, at 100kg (which is 70kg for the payload and 5kg per rod) in order to highlight the impact of structural geometry and rod length. For the tension members we used spring constants of 44 kN/m for the cables around the perimeter and 10 kN/m for the cables attached to the payload. Also, the results in Figure 10 were found using the landing orientation of 35 degrees around X axis and 45 degrees around Z axis, which we selected from our orientation studies discussed below.

A very interesting point to consider is that the mass of our system will grow in a linear fashion with the length in the rods, while providing increasing payload protection. On the other hand, the mass of airbags increases with the square of the radius, which is one of the reasons that the MSL rover, with its increased size and mass, had to switch from the airbag approach used by MSL to the more complex Sky Crane approach. While this study has focused on small light-weight mission concepts, we expect that there are compelling advantages to scaling up to handle larger payloads and we look forward to studying this further in the future.

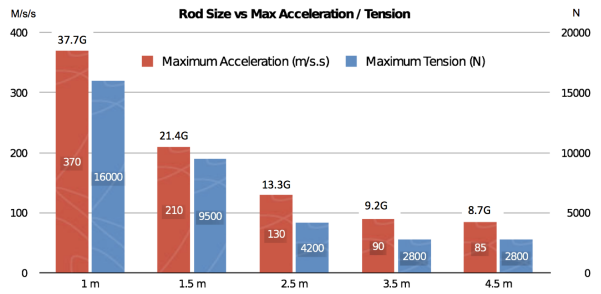

Figure 10: **Landing Forces Study**. *This shows how rod length impacts maximum deceleration of the payload and the maximum forces experienced by the tension cables. All tests were conducted with a landing velocity of 15 m/s onto a hard surface.*

4.5. Landing Orientation Studies

In order to study how landing orientation affects payload decelerations and impact events, we conducted a systematic study of landing orientations. Since we wanted to get meaningful data, even for bad orientations, we used a larger tensegrity with 4 meter rods so the data wouldn't saturate. Our success criteria for this study was that the decelerations had to stay under an upper limit of 25G deceleration of the payload, and the payload had to avoid collision with the ground or parts of the tensegrity structure. Figure 11 shows the orientations that were safely within these criteria (black) or failed one or both of the criteria (colored). By using a simple trailing streamer during descent it would be possible to control landing at an optimal orientation and enable the use of smaller structures with shorter rods because the orientation control would maximize the available stroke for the payload to decelerate within the structure. Conversely, we can use these studies to know what the worst possible landing scenario will be and choose a structure size which will allow safe landing at any orientation.

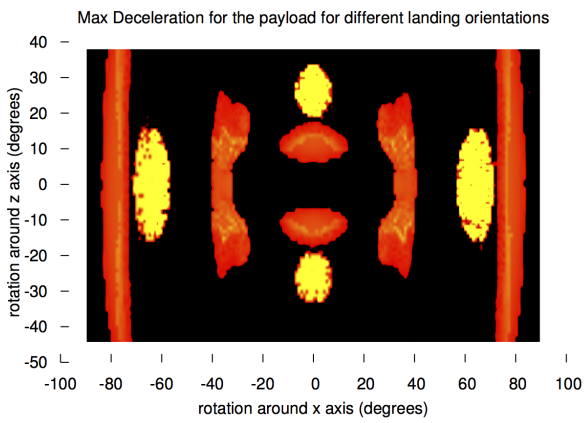

Figure 11: *Heat map of the maximum acceleration that the payload encounters for all possible landing orientations. Black areas are safe, colored areas are where the payload does not meet one or both success criteria.*

4.6. Conclusions from Simulation Experiments

In our landing analysis we developed and cross-validated two different simulation methods that allowed us to explore the capabilities of a tensegrity structure to absorb the forces of landing and to simultaneously protect a delicate payload. This analysis confirmed that indeed it is possible to do so using a 6-bar tensegrity probe while maintaining maximum decelerations experienced by the instrument-containing payload to forces less than 25G, despite the structure landing at 15 m/s (which is greater than terminal velocity on Titan). Comparing this to the Huygens probe's landing acceleration of $32G$ [25], the tensegrtiy probe will have a 43% reduction in G forces experienced by the scientific payload, despite the Huygens probe's use of parachutes to land at 1/3 of the speed of our tensegrity probe.

5. PROTOTYPE HARDWARE FOR DEPLOYMENT AND DROP TESTS

Having calibrated our two simulators to each other and shown that our structure could protect a payload during landing at Titan terminal velocity, we built a hardware prototype to confirm that our simulations and analytics were reasonable. The first prototype we constructed was intended to show the ability to be deployed from a packed configuration, to survive a landing at Titan terminal velocity (11 m/s, which is equivalent to a 10m drop test terrestrially), and to then still be functional as demonstrated by re-stowing and re-deploying. As a fast, cheap, first experiment at surviving landing at 11 m/s, we choose to use the minimal amount of actuators to accomplish our goals and were not trying to optimize weight, payloads, or to demonstrate rolling mobility, which are issues for a future investigation.

5.1. Structure

The prototype show in Figure 12 is constructed of 1-3/8" OD, 1/8" wall thickness aluminum, cut into 20 inch long rods. This diameter was chosen so that the motors and controllers could be embedded within the rods for protection during landing. Instead of actuating all 24 tension members, as desired for mobility and the compact storage shown in Figure 3, we placed one actuator in each rod such that six strings were actuated and the other 18 elements were passive springs. This is the minimal amount of actuation required for a reasonably compact storage configuration, as discussed below. For the six actuated connections, 200 lb test Dacron string was used, with a short strong spring at the attachment to provide some compliance. For the 18 passive members, extension springs with a spring constant (k) equal to 1.5 lbs/in were selected after testing springs rates of 0.5 lbs/in and 0.7 lbs/in. All connections were held in place by threading $1/4$"-28" holes on both ends of each strut and fitting them with steel spring anchors.

Figure 12: Prototype Probe

5.2. Motor Implementation

To mechanize the movement of the structure from standing to a collapsed position and back to a standing position six Pololu 172:1 metal DC gearmotors were internally mounted. Three in the ends of each strut that form one of the equilateral triangular faces with three more motors in the opposite side of the structure again forming an equilateral triangular face. Each motorized end assembly has the motor fitted in an aluminum sleeve with diameter a couple hundredths less than that of the aluminum pipe for a tight fit. 10-32 set screws were joined into the rod and pressed down onto the sleeve to hold the motor in place. On the top shaft of each motor a spool was placed and locked in place with a 4-40 set screw. Figure 13 below shows an exploded view of this motorized end assembly.

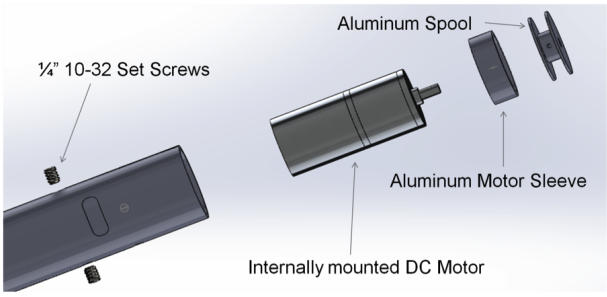

Figure 13: Assembly of actuators into the Rods of the the prototype lander

5.3. Storage and Deployment

Given the limited actuation of the prototype we found two methods of collapsing and expanding the structure, of which the most efficient was the Star configuration. This packing approach requires an orientation where the actuated faces are the top and bottom of the structure. By rotating the motors such that the sting faces are allowed to elongate, the structure will collapse into a relatively flat star shape as shown in Figure 14. The final height of this method depends on the diameter of the springs as they prevent it from packing flat. Looking at this image, one can see that with more actuation, the rods of the top triangle could be pulled into place for optimal packing. From this configuration, there was no trouble re-deploying to full standing in preparation for the Drop Tests.

Figure 14: Prototype packed almost flat in the the Star Configuration

5.4. Prototype Drop Tests

Once the prototype was built and deployment demonstrated, a series of drop tests were performed from successively greater heights until 10m (30') was reached, at which point the prototype was landing at around 11 m/s, which is comparable to the terminal landing speed expected on Titan. After landing, the test was shown to be successful by demonstrating that the lander still functioned and could be collapsed to its packed state and once more deployed. In Figure 15 we show a sequence from the 7.5m drop test. During this landing, the probe rebounded and rolled sideways a distance about twice its diameter.

Most significantly, the probe survived the 10m (30') drop test and was still functional afterwards, giving us confidence that this approach is viable, and that our simulation results are accurate enough to proceed to further analysis. One useful insight from this test is that the motors unspooled (i.e. were back driven) by a few centimeters during the landing. Thus, it is recommended that brakes be integrated to the motors, so they can be mechanically locked in place during landing.

Figure 15: Drop test from 7.5m.

Figure 16: Drop test from 10m (30') – equivalent to terminal velocity on Titan

6. SURFACE MOBILITY

Tensegrity robots have the potential to be fabulous mobility platforms as they can be light-weight, energy efficient, robust against failures, and can traverse across unfavorable terrains. However controlling these robots is difficult since there are many points of control, the controls interact in non-linear ways, and the structure as a whole is oscillatory. Using traditional control algorithms for mobile tensegrity robots is difficult and previous successful attempts have been limited to very slow static gaits, and evolutionary control of very simple structures. Fortunately we have had tremendous success with evolutionary algorithms and later with dynamical and Central Pattern Generator based controls (see Figure 17) for generating fast and efficient rolling motions in our tensegrity probe. This work has been extensively reported on in other papers (see [16, 18, 19]), and is briefly summarized here.

We performed several tests of evolutionary control in the NTRT simulator. Using open loop control, the evolutionary algorithm is able to find a control policy that allows the tensegrity robot to roll quickly in a smooth manner. These results were robust to adding small obstacles to the terrain and was even able to keep rolling after we cut one of the control cables.

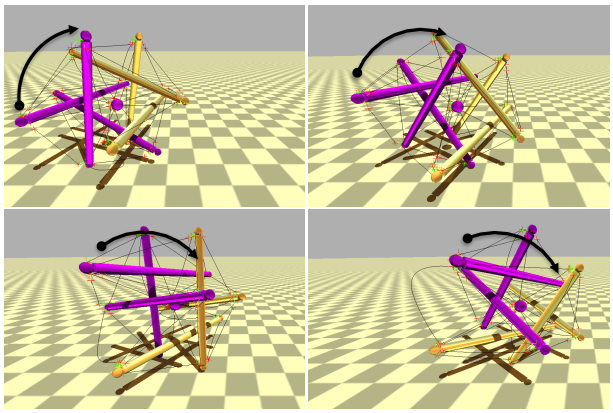

Figure 17: **Tensegrity Dynamics**. *Tensegrity is able to achieve smooth rolling motion. This rolling is accomplished solely by changing the length of the cables. Our learned control policies produce rolling that is also dynamical as the tensegrity does not stop to setup next roll action. This type of rolling can be fast and highly efficient.*

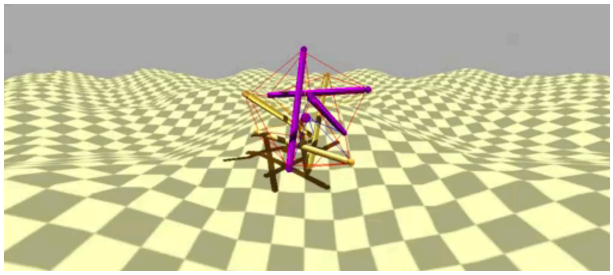

Figure 18: **Dynamical and Central Pattern Generator Based Control**. *Our dynamical controls allows tensegrity to climb over moderate hills.*

The controls used by our evolutionary methods were a simple form of semi-distributed oscillatory control: All the actuations were controlled through sine waves synchronized through their relative phase shifts. These controls proved to be robust and sufficient for our goals of having our tensegrity platform roll smoothly. These controls also gave excellent examples and insight into what fundamental dynamics were required for fast smooth motion. On the other hand, these controls are open-loop and as a result, a major limitation of these evolved controls is that they do not provide a means to direct or steer the motion of the tensegrity probe. Rather, a control law is learned which can be abstracted, but which does not allow reactive changes of direction. To develop steerable controls we took the insights gained from the evolved controllers and hand crafted reactive dynamical controllers that used a variety of simulated sensor feedbacks to enable steerable rolling. This approach was very successful and was shown to work on a variety of terrains, including moderate hills (Figure 18). But, this approach relied on significant amounts of sensor feedback which may be difficult to implement, so we wanted to find a hybrid approach that enabled steering while using a minimum amount of sensor feedback. Central Pattern Gener-

ators (CPG's) are able to store complex gait cycles in their network dynamics allowing for a significant reduction of sensor feedback required. We explored a variety of ways to use this property and to combine it with aspects of the dynamical controls approach to enable steering. The best result found so far uses the hand-coded dynamical controller as a trainer to learn the parameters for a Hybrid CPG which combines Hopf oscillators and Inverse Kinematics. Details of this approach can be found in [2].

7. CONCLUSIONS

Using multiple analysis and simulation tools we showed that tensegrities are a very robust landing platform, and can protect delicate payloads from a landing impact of 15 m/s (and possibly beyond). This was further confirmed by performing drop tests on multiple physical prototypes. Combined with our investigations of packing, deployment, and mobility, we thus show that tensegrity probes can be effective landing and mobility platforms for a Titan mission. Compared to existing flown missions, a tensegrity probe can have a high mass fraction between science payload and overall weight (as measured at atmospheric entry) due to its dual use as a landing system (like an airbag) and as a system for surface mobility. As a result, tensegrity based missions can be cheaper and open up new forms of surface exploration that take advantage of their natural tolerance to impacts.

ACKNOWLEDGMENTS

The work presented here was primarily supported by funding from the NASA Innovative Advanced Concepts (NIAC) Program. For the physical drop tests, we thank Mogley Samter, Sarah Lynn, Karen Jolley, Joe Hepner, Kyle Morse, and Nathan Clark from the University of Idaho and the Idaho Space Grant Consortium which supported their work. The E-L simulator was initially developed by Ken Caluwaerts, from Ghent University, Belgium. Finally, we are deeply grateful to Terry Fong and the NASA Ames Intelligent Robotics Group (IRG) for their on-going support of our tensegrity research.

REFERENCES

[1] NASA Tensegrity Robotics Toolkit (NTRT), open source release information available at: https://ti.arc.nasa.gov/dev/tech/asr/intelligent-robotics/tensegrity/.

[2] A. Agogino, V. SunSpiral, and D. Atkinson. Super ball bot - structures for planetary landing and exploration. *NASA Innovative Advanced Concepts (NIAC) Program, Final Report*, 2013.

[3] J. B. Aldrich and R. E. Skelton. Backlash-free motion control of robotic manipulators driven by tensegrity motor networks. *IEEE Conference on Decision And Control*, pages 2300–2306, 2006.

[4] T. Bliss. Central pattern generator control of a tensegrity swimmer. *Ph.D. thesis, Dept. Mech. Aerosp. Eng., Univ. Virginia,*, Dec. 2011.

[5] T. Bliss, J. Werly, T. Iwasaki, and H. Bart-Smith. Experimental validation of robust resonance entrainment for CPG-controlled tensegrity structures. *IEEE Transactions On Control Systems Technology*, 2012.

[6] T. K. Bliss, T. Iwasaki, and H. Bart-Smith. CPG Control of a Tensegrity Morphing Structure for Biomimetic Applications. *Advances in Science and Technology*, 58:137–142, 2008.

[7] V. Böhm, A. Jentzsch, T. Kaufhold, F. Schneider, and K. Zimmermann. An approach to compliant locomotion systems based on tensegrity structures. *56th International Scientific Colloquium, Ilmenau University of Technology*, pages 1–6, Aug. 2011.

[8] K. Clausen, H. Hassan, M. Verdant, P. Couzin, G. Huttin, M. Brisson, C. Sollazzo, and J.-P. Lebreton. The huygens probe system design. In *The Cassini-Huygens Mission*, pages 155–189. Springer, 2003.

[9] R. Connelly and A. Back. Mathematics and tensegrity: Group and representation theory make it possible to form a complete catalogue of" strut-cable" constructions with prescribed symmetries. *American Scientist*, 86(2):142–151, 1998.

[10] M. Darrach, R. Kidd, J. MacAskill, A. Chutjian, J. Simcic, E. Neidholdt, M. Sinha, and B. Bae. An overview of mass spectroscopy based instrument development at the jet propulsion laboratory. mr. *LPI Contributions*, 1683:1114, 2012.

[11] R. B. FULLER. Tensile-integrity structures, Nov. 13 1962. US Patent 3,063,521.

[12] M. P. Golombek. The mars pathfinder mission. *Journal of geophysical research*, 102(E2):3953–3965, 1997.

[13] J. Gomez-Elvira and R. Team. Environmental monitoring station for mars science laboratory. *LPI Contributions*, 1447:9052, 2008.

[14] K. Herkenhoff, S. Squyres, J. Bell III, J. Maki, H. Arneson, P. Bertelsen, D. Brown, S. Collins, A. Dingizian, S. Elliott, et al. Athena microscopic imager investigation. *Journal of Geophysical Research*, 108(E12):8065, 2003.

[15] D. E. Ingber. The architecture of life. *Scientific American*, 278(1):48–57, 1998.

[16] A. Iscen, A. Agogino, V. SunSpiral, and K. Tumer. Controlling tensegrity robots through evolution. In *Genetic and Evolutionary Computation Conference (GECCO 2013)*, Amsterdam, NL, 2013.

[17] A. Iscen, A. Agogino, V. SunSpiral, and K. Tumer. Learning to control complex tensegrity robots. In *To appear in: Twelfth International Conference on Autonomous Agents and Multiagent Systems*, 2013.

[18] A. Iscen, A. Agogino, V. SunSpiral, and K. Tumer. Learning to control complex tensegrity robots. In *Proceedings of the 2013 International Conference on Autonomous Agents and Multi-Agent Systems*, AAMAS '13, pages 1193–1194, Richland, SC, 2013. International Foundation for Autonomous Agents and Multiagent Systems.

[19] A. Iscen, A. Agogino, V. SunSpiral, and K. Tumer. Robust distributed control of rolling tensegrity robot. In *The Autonomous Robots and Multirobot Systems (ARMS) Workshop at AAMAS 2013*, 2013.

[20] Y. Koizumi, M. Shibata, and S. Hirai. Rolling Tensegrity Driven by Pneumatic Soft Actuators. *Robotics*, pages 1988–1993, 2012.

[21] B. Laub and E. Venkatapathy. Thermal protection system technology and facility needs for demanding future planetary missions. In *International Workshop on Planetary Probe Atmospheric Entry and Descent Trajectory Analysis and Science*, pages 268–278, Oct 2003.

[22] D. Lee. The mission loads environment and structural design of the mars science laboratory. 2012.

[23] S. M. Levin. The tensegrity-truss as a model for spine mechanics: biotensegrity. *Journal of Mechanics in Medicine and Biology*, 2:375–388, 2002.

[24] M. K. Lockwood, E. M. Queen, D. W. Way, R. W. Powell, K. Edquist, B. W. Starr, B. R. Hollis, V. E. Zoby, G. A. Hrinda, and R. W. Bailey. Aerocapture Systems Analysis for a Titan Mission. Technical report, NASA Langley Research Center, Feb 2011.

[25] R. Lorenz. Huygens probe impact dynamics. *ESA Journal*, 18:93–117, 1994.

[26] J. Maki, D. Thiessen, A. Pourangi, P. Kobzeff, L. Scherr, T. Elliott, A. Dingizian, and B. St Ange. The mars science laboratory (msl) navigation cameras (navcams). In *Lunar and Planetary Institute Science Conference Abstracts*, volume 42, page 2738, 2011.

[27] M. Masic and et al. Algebraic tensegrity form-finding. *International Journal of Solids and Structures*, 42:4833–4858, 2005.

[28] M. Masic and R. E. Skelton. Open-loop control of class-2 tensegrity towers. *Proceedings of the 11th Smart Structures and Materials Conference*, 5383:298–308, 2004.

[29] J. M. Mirats-Tur. On the movement of tensegrity structures. In *International Journal of Space Structures*, volume 25, 2010.

[30] K. W. Moored, III, S. A. Taylor, and H. Bart-Smith. Optimization of a Tensegrity Wing for Biomimetic Applications. *Proceedings of SPIE*, 6173:617313, Mar. 2011.

[31] E. N. Nilsen. Exploring mars: an overview. 2012.

[32] O. Orki. *A Model Of Caterpillar Locomotion Based On Assur Tensegrity Structures*. PhD thesis, Tel Aviv University, 2012.

[33] O. Orki, A. Ayali, O. Shai, and U. Ben-Hanan. Modeling of caterpillar crawl using novel tensegrity structures. *Bioinspiration & Biomimetics*, 7(4):046006, 2012.

[34] O. Orki, O. Shai, A. Ayali, and U. Ben-Hanan. A Model of Caterpillar Locomotion Based on Assur Tensegrity Structures. *Proceedings of the ASME 2011 IDETC/CIE*, Aug. 2011.

[35] C. Paul, H. Lipson, and F. J. V. Cuevas. Evolutionary form-finding of tensegrity structures. *Proceedings of the 2005 Genetic and Evolutionary Computation Conference (GECCO)*, pages 3–10, 2005.

[36] C. Paul, J. W. Roberts, H. Lipson, and F. J. V. Cuevas. Gait production in a tensegrity based robot. In *Advanced Robotics, 2005. ICAR '05. Proceedings., 12th International Conference on*, Jan. 2005.

[37] C. Paul, F. J. Valero-Cuevas, and H. Lipson. Design and control of tensegrity robots for locomotion. *IEEE Transactions on Robotics*, 22(5), Oct. 2006.

[38] S. Pellegrino. *Mechanics of kinematically indeterminate structures*. PhD thesis, University of Cambridge, 1986.

[39] A. Pugh. *An introduction to tensegrity*. Univ of California Press, 1976.

[40] S. R, T. W. Findley, L. Chaitow, and P. Huijing, editors. *Fascia: The Tensional Network of the Human Body: The science and clinical applications in manual and movement therapy, 1e*. Churchill Livingstone, 1 edition, Apr. 2012.

[41] J. Rieffel, R. Stuk, F. Valero Cuevas, and H. Lipson. Locomotion of a Tensegrity Robot via Dynamically Coupled Modules. *Proceedings of the International Conference on Morphological Computation*, 2007.

[42] J. Rieffel, B. Trimmer, and H. Lipson. Mechanism as Mind : What Tensegrities and Caterpillars Can Teach Us about Soft Robotics The Manduca Sexta Caterpillar : Morphological Communication in Tensegrity Robots. *Artificial Life*, pages 506–512, 2008.

[43] J. A. Rieffel, F. J. Valero-Cuevas, and H. Lipson. Morphological communication: exploiting coupled dynamics in a complex mechanical structure to achieve locomotion. *Journal of the Royal Society, Interface / the Royal Society*, 7(45):613–21, Apr. 2010.

[44] M. Shibata and S. Hirai. Rolling Locomotion of Deformable Tensegrity Structure. *Mobile Robotics: Solutions and Challenges*, pages 479–486, 2009.

[45] M. Shibata, F. Saijyo, and S. Hirai. Crawling by body deformation of tensegrity structure robots. In *Robotics and Automation, 2009. ICRA '09. IEEE International Conference on*, pages 4375 –4380, may 2009.

[46] R. Skelton. Dynamics and control of tensegrity systems. In H. Ulbrich and W. Gnthner, editors, *IUTAM Symposium on Vibration Control of Nonlinear Mechanisms and Structures*, volume 130 of *Solid Mechanics and its Applications*, pages 309–318. Springer Netherlands, 2005.

[47] R. E. Skelton and M. C. De Oliveira. *Tensegrity Systems*. Springer, 2009 edition, June 2009.

[48] R. E. Skelton and M. C. Oliveria. *Tensegrity Systems*. Springer, New York, 2009.

[49] K. Snelson. http://www.kennethsnelson.net/.

[50] K. Snelson. Continuous tension, discontinuous compression structures. united states patent 3169611, Feburary 1965.

[51] Tibert and et al. Review of form-finding methods for tensegrity structures. *International Journal of Space Structures*, 18:209–223, 2003.

[52] A. Tibert and S. Pellegrino. Review of form-finding methods for tensegrity structures. *International Journal of Space Structures*, 18(4):209–223, 2003.

[53] B. R. Tietz, R. W. Carnahan, R. J. Bachmann, R. D. Quinn, and V. Sunspiral. Tetraspine : Robust Terrain Handling on a Tensegrity Robot Using Centr al Pattern Generators. In *2013 IEEE/ASME Advanced Intelligent Mechatronics*. IEEE, July 2013.

[54] J. M. M. Tur and S. H. Juan. Tensegrity frameworks: Dynamic analysis review and open problems. *Mechanism and Machine Theory*, 44:1–18, 2009.

[55] J. Y. Zhang and M. Ohsaki. Adaptive force density method for form-finding problem of tensegrity structures. *International Journal of Solids and Structures*, 43:5658–5673, 2006.

[56] L. Zhang and et al. Form-finding of nonregular tensegrity systems. *Journal of Structural Engineering*, 132:1435–1440, 2006.